Microscopic observation of miscible mixing in sprays at elevated temperatures and pressures

J. Manin[*] and L. M. Pickett
Combustion Research Facility
Sandia National Laboratories
Livermore, CA 94550 USA
C. Crua
Centre for Automotive Engineering
University of Brighton
Brighton BN2 4GJ, United Kingdom

Abstract

Recent visualization of n-dodecane delivered from a diesel injector into environments above 60 bar and 900 K performed at Sandia National Laboratories suggested a reduction in surface tension as droplets and ligaments were no longer detectible via back-illuminated microscopy. In the current study, improvements in optical microscopy are implemented to overcome much of the optical distortion present at these harsh conditions, leading to greater measurement resolution. The measurements show that the classical atomization and vaporization processes do shift to one where surface tension forces diminish with increasing pressure and temperature. Key indicators of "miscible mixing" include a deformation of liquid structure under minimal shear from surrounding gas velocities as well as indications that both large-scale turbulent motions and local molecular diffusivity simultaneously drive the mixing between fluids of different densities. A new fundamental finding of this study is that the transition to miscible mixing does not occur instantaneously when the fluid enters the chamber at a given temperature and pressure where miscible mixing is observed. Rather, the large, cool liquid structure that was just injected exhibits surface tension at first, and then, after time surrounded by the hot ambient and other fuel vapor, undergoes a transition to miscible mixing.

[*]Corresponding author: JManin@sandia.gov

Introduction and background

Mixing of liquid fuel with ambient gases is critical to combustion and emission performances in thermal engines. A variety of experimental approaches and high-fidelity computational fluid dynamic (CFD) efforts are underway to help understand the physical processes that drive this mixing. Ultimately, advanced models with sensitivity to the key physics are needed to calibrate engineering codes that designers use to optimize engine development.

The situation of cold liquid fuel injected into gas at very high pressure and temperature conditions creates special challenges in this respect. The fuel inside the nozzle is highly pressurized, but below its critical temperature, and it is then injected into thermodynamic conditions above the critical point of the fuel. Different thermodynamic phase diagrams may be generated for the fuel, or the ambient, or mixtures of fuel and ambient at a given mixture fraction [1], and one is shown with respect to the fuel in Figure 1 simply to represent the injection process schematically in pressure – temperature space. Considering typical fuels injected into diesel engines, the fuel critical point is around 20 bar in pressure and close to 700 K in temperature. The ambient gas conditions easily exceed this temperature for normal operation inside the combustion chamber of diesel engines: the Spray A case of the Engine Combustion Network (ECN) for example, prescribes 60 bar and 900 K [2]. Fuel may enter the chamber as a cool, compressed liquid, but its temperature will increase as it mixes with the hot ambient. While there is potential for the liquid to exhibit "supercritical" or "transcritical" tendencies, with reduced surface tension, this is not a single-phase system and the important question is how the interface between cold liquid fuel and hot ambient responds at the pressures and temperatures specific to engines.

Understanding the mixing behavior of different fluids at high pressure and temperature has therefore been pursued in different experimental and computational research programs [3]. For example, injection of cryogenic liquid and oxygen constitutes a focus area for the liquid rocket community [4]. Recent efforts have also addressed the thermodynamic conditions of relevance for internal combustion engines [1, 5, 6]. Gradient theory modeling research by Dahms et al. [1, 5] shows that the interface between liquid fuel and vapor ambient gases tends to broaden at high-pressure and high-temperature conditions, reducing surface tension and allowing the mixture to enter a continuum where diffusive transport properties dominate over inter-molecular forces. Essentially, the mixing processes change and there is less evidence of surface tension. Experiments carried out by Manin et al. [6] and Falgout et al. [7]

support the detailed thermodynamic analysis from Dahms et al. [1] by visualizing the mixture formation of n-dodecane sprays into high-pressure, high-temperature environments. However, the images suffered from degradation because of the pressurized and heated environments, preventing a direct measurement of the fuel-ambient interfacial region and leaving uncertainty in the experimental conclusions. High-resolution experiments, particularly time-resolved measurements, where the physics of mixing of liquid structures can be diagnosed even if not fully resolved, are still needed to unveil the physics of the different mixing processes when diffusion contributes to the global mixing field.
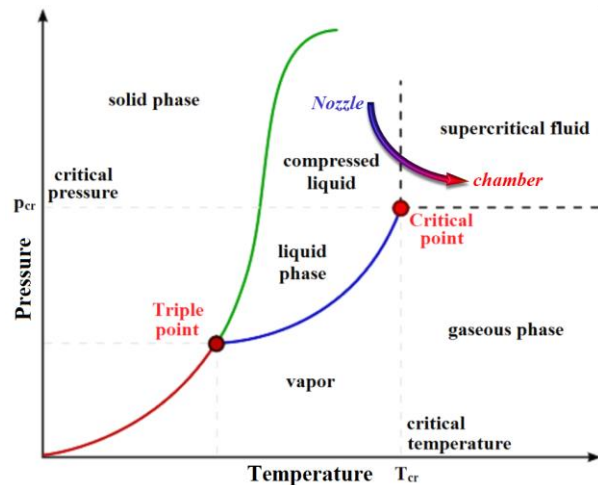
Figure 1. Pressure-Temperature phase diagram of a transcritical mixing process under realistic engine conditions. Triple and critical points correspond to the fuel properties.

Evidence that the time history of the mixture is important has come from recent work by Dahms and coworkers [8]. Progressing beyond an analysis of the vapor – liquid interface at equilibrium [1], a non-equilibrium analysis shows that surface tension does not vanish instantly. Rather, the authors found that the interface thickens in time beyond the equilibrium solution, favoring the reduction in intermolecular forces, i.e., surface tension.

In this experimental paper, we implement an improved microscopic setup with high-speed visualization capability to track droplets and liquid structures in liquid sprays injected into high-temperature, high-pressure environments. The objective is to find evidence of surface tension in the system, or a transition to "miscible mixing" between the fuel and ambient gases where surface tension forces diminish.
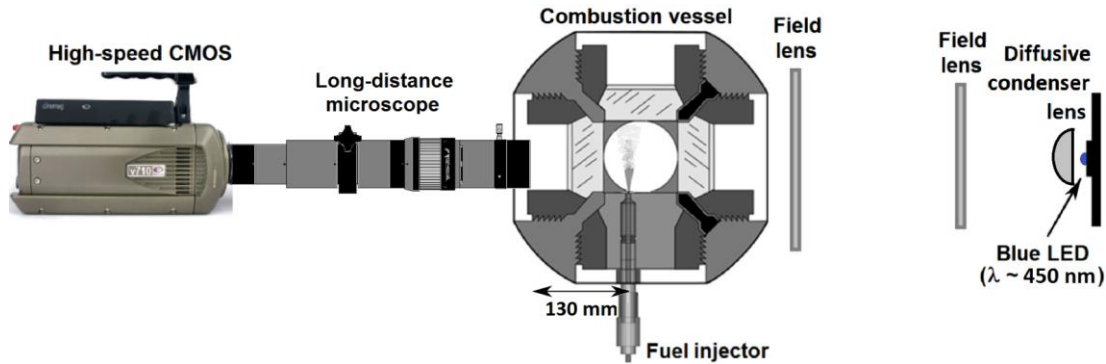
Figure 2. Optically accessible spray vessel (center), high-speed long-distance microscopic imaging system (left) and LED-based diffused back-illumination system (right).

The remaining of the manuscript first describes the experimental installations and the specifics of the experiments. The results are presented next, featuring image sequences extracted from high-speed movies showing the mixing processes under different operating conditions. The last section summarizes the conceptual findings and lays out further efforts in this topic.

Experimental apparatus

Optically accessible vessel and injection system
An optically accessible vessel capable of simulating high-temperature and high-pressure environments up to 35 MPa and 1400 K has been used for these experiments. The constant-volume chamber is pre-heated to 188°C during operation and the thermodynamic conditions are reached by ignition and combustion of reactants composed of C_2H_2, H_2, N_2 and O_2. After spark ignition and combustion and a relatively long cooldown period for the ambient gases, the injection event is triggered when the gases reach a particular temperature and pressure. The vessel is nearly of cubical shape, and offers a fully modular configuration regarding the six faces and eight corners of the chamber. In these experiments, two sapphire windows were fitted into the ports located on either side of the injector, another sapphire window was used in the port facing the injector. The other faces were fitted with the injector port, the spark plugs and a metal port. The corners were fitted with two intake and one exhaust valves, two pressure transducers, a thermocouple and a stirring fan, with the last corner being plugged (unused). A schematic of the experimental arrangement is depicted in Figure 2, showing the spray vessel in the middle with the two optical windows to accommodate the line-of-sight imaging setup described later.

The sprays were injected via a solenoid-actuated common-rail injector equipped with an axially-drilled single-hole nozzle. The diameter of the nozzle was 0.180 mm and the orifice features a converging conical shape (*K-factor* = 1.5). The port into which the injector is fitted is equipped with a temperature-regulated liquid-cooled system, which maintains the temperature of the injector tip around 90°C during operation [9]. The fuel was pressurized via an air-driven high-pressure fuel pump, and supplied to the injector via high-pressure fuel lines, connections and a commercially available common-rail. The experimental results presented in the next section only feature visualizations performed with an injection pressure of 50 MPa. A lower injection pressure was purposely selected to generate a broad droplet size distribution at lower velocities, especially during the end of injection. Three fuels were used as the injected fluid: N-heptane, n-dodecane and n-hexadecane. The ambient temperature and pressure were varied from approximately 2 to 11 MPa, and the temperature from 700 to 1200 K.

Optical setup
The optical system was composed of a high-speed camera equipped with a long-distance microscopic lens for the imaging part and a LED-based system as illumination source. Diffused back-illumination was used to produce a uniform light distribution and compensate for beam-steering activity produced by the high ambient pressure in the chamber. The diffused back-illumination arrangement was optimized toward microscopy and was composed of a diffusive aspherical condenser lens (25 mm diameter, 20 mm focal length) to efficiently collect and diffuse the LED light, followed by two Fresnel lenses of 75 and 150 mm focal lengths, in that order. This combination of lenses relays the image of the diffusive surface of the condenser lens onto the imaging plane, corresponding to the spray axis. Even though the LED system is capable of light pulses shorter than 10 ns, the pulse duration was set to 200 ns during these experiments to provide sufficient light intensity. This is another reason to use the lower injection pressure mentioned earlier, as the flow is slowed down. It must be

noted that most of the observations have been made during or after the end of injection, when the flow velocities are significantly reduced with respect to the main injection period. The LED source used during these experiments was a high-flux royal blue, with an illumination spectrum center around 450 nm.

The high-speed CMOS camera was run at full frame (1024 x 1024 pixels), with frame rates ranging from 10000 to 18000 frames per second (fps). The relatively low camera acquisition rate was chosen to favor the largest field of view, at any given magnification. Because most of the qualitative analysis can only be performed at timings when flow velocities are reduced, the imaging acquisition frequencies were appropriate to temporally track flow features during these timings. The camera exposure time was set to 2 µs, but the effective imaging exposure time was set by the illumination duration of approximately 200 ns. The long-distance microscopic objective mounted onto the high-speed camera provided two magnification powers during these measurements: 2x and 8x. The digital resolutions of the images were respectively 10 and 2.5 µm per pixel, providing a Nyquist resolution-limited frequency of approximately 55 and 230 cycles/mm, in that order. The numerical aperture of the system was 0.16 (corresponding to a collection angle of approximately 320 mrad). It can be noted that the diffraction-limited image resolution of the microscope for this configuration was below 2 µm, or less than a pixel.

Characterization and calibration

As detailed by Manin et al. [6], capturing microscopic images of potentially unknown features in highly pressurized environments is complicated. For the measurements to provide any insightful information, the degradation in image quality, if any, needs to be carefully evaluated and quantified. The magnitudes associated with image quality needs to be related to physical quantities such as length scale. The criterion proposed by Manin and coworkers [6] correlates image degradation with a microscopic length scale by providing an equivalent circle-of-confusion. In that context, the circle-of-confusion indicates the size of the minimum resolvable feature by the imaging system for any particular image sequence.

The modulation transfer function (MTF) of an optical system is another parameter that quantifies image sharpness through the image contrast as a function of frequency, i.e., line pairs per millimeter (lp/mm). The MTF can easily be obtained by measuring the response of the system to a knife-edge for instance. Transforming the derivative of the knife-edge slope response into the frequency domain provides the MTF of the system under this condition. This method is similar to the one used by Manin et al. [6] to extract the equivalent circle-

of-confusion, through another parameter that the authors called the contrast quality factor. For comparison with the MTF, the contrast quality factor simply provides the resolvable image frequency (i.e., MTF) at a specific contrast considered as the low limit $(1/e^2)$ based on background image noise.

The MTF of the system for the two magnification power cases applied are plotted in Figure 3. These measurements were made on the bench, without the limitations and complexities of the combustion chamber. They can therefore be considered as the best possible response from the imaging system under ideal conditions.
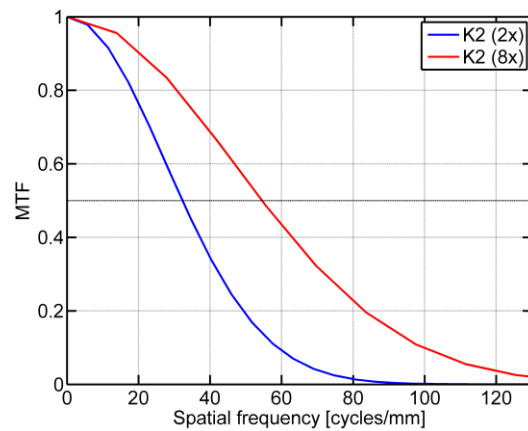
Figure 3. Modulation transfer function (MTF) of the microscopic imaging system (K2) for the 2 and 8x magnification configurations used in the experiments.

The MTF at 50 % contrast is commonly used to quote a single quantity rather than the entire contrast range. The measurements reported in Figure 3 show that the MTF magnitudes at 50 % contrast were 32 and 55 cycles/mm for the 2 and 8 magnification powers, respectively. These results are somewhat surprising because the magnification ratio is a factor four between the two levels, but the resulting improvements in image resolution did not even double. The most likely explanation for the non-linear resolution improvement with magnification is the limited numerical aperture of the system (0.16). Even though the theoretical resolution of the system based on the Abbe criterion is below 2 µm, wave optics limitations, such as diffraction for instance, also affects the system's response for increasing frequencies.

The depth of field of a microscopic imaging arrangement is of crucial importance when studying three-dimensional systems like a turbulent flow field. Thanks to the long-distance microscopic objective used in this work, the depth of field of the optical system is

relatively longer than typical microscopes of similar magnification levels. Tests were conducted to evaluate the depth of field of the optical system and the degradation of the images in terms of MTF. The results showed that features with dimensions similar to the droplets tracked in the experiments were detected by the imaging systems within about 200 µm around the best focal position on benchtop experiments. However, significant deviations arise when visualizing features in a high-temperature, high-pressure environment. Under these conditions, large and sharp density gradients steer the light rays in different directions by modifying the refractive index distribution within the pressure vessel. The fluctuating temperature field within the vessel induces unpredictable refractive index gradients that randomly affect the images in time and space. The tests performed under relevant thermal engine conditions used a tilted Ronchi ruling featuring a 20 lp/mm pattern. The time-resolved imaging data during the typical chamber operation described earlier demonstrated the difficulty encountered when visualizing through pressurized and heated gases. During the pre-burn and cooldown periods, the focal plane position moves significantly, while image quality is severely degraded. Work is ongoing to report the full characterization of the system as well as to provide guidance regarding quantitative assessment of image quality under pressurized and heated environments. Nevertheless, the tests provided the information necessary to limit the range of droplets or fluid structures to be tracked during the experiments: Droplets or features larger than 30 µm were identified and tracked, while smaller structures were generally not treated.

Results and discussions

To present the spray system from a global point of view, a relatively large field of view (around 10 mm long) is imaged first. The images displayed in Figure 4 present sample back-illuminated images extracted from the high-speed movies taken during the end of injection period. The high-speed videos of the sequences presented in this manuscript are available in the data archive of the ECN website [2]. The 2x magnification configuration was used to acquire high-speed images of the extended near-nozzle region. The large field of view, combined with the relatively high optical resolution (digital resolution: 10 µm/pix) allows tracking of the spray features and droplets generated by the end of injection flow. In these sequences, the injector is located on the left, and the spray exits the axially-drilled nozzle orifice penetrating horizontally to the right on the images. A simple intensity normalization has been performed on the image to keep the image intensities and contrasts to similar levels across the different acquisitions. Figure 4 displays two sequences of three images taken at different timing from the end of injec-

tion to approximately 1.5 ms after the end of the injection event. In the images of Figure 4A, n-hexadecane fuel is injected at 50 MPa into an ambient held at 900 K temperature and 60 bar pressure. This condition corresponds to the ambient density of 22.8 kg/m^3 and matches the Spray A case of the ECN, introduced earlier, thus highlighting the relevance to diesel engine combustion. Note that the Spray A condition prescribes n-dodecane as the fuel and a higher fuel injection pressure of 150 MPa. N-hexadecane certainly is the most representative surrogate alkane fuel for diesel from a physic-chemical point of view. The sequence of Figure 4B features n-hexadecane as well, also injected at 50 MPa, but into a hotter and denser environment of 1200 K in temperature and 105 bar in pressure (30.4 kg/m^3 density). This condition is still highly relevant to modern boosted engines, especially when the fuel is injected at or past top-dead-center, or after the start of combustion. Note that the timings displayed in Figure 4 for both sequences are matched to show the spray process at similar stages after injection.
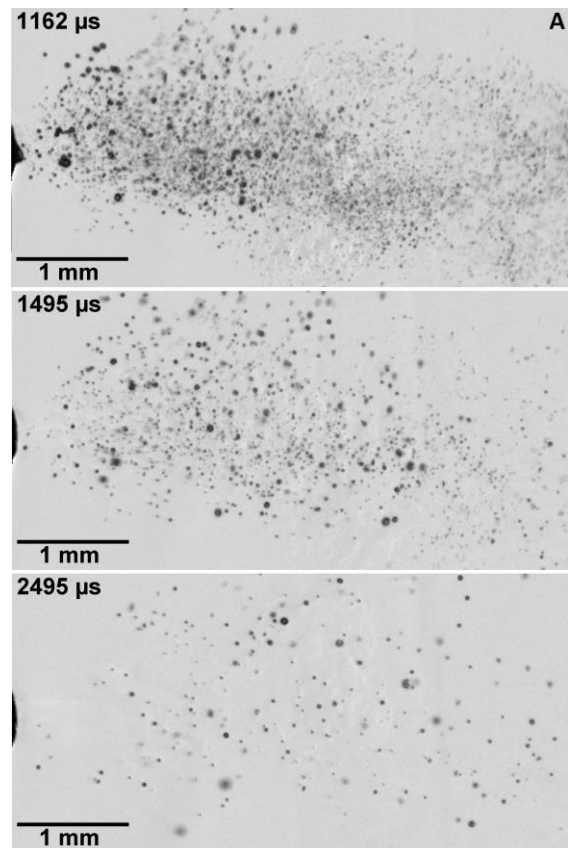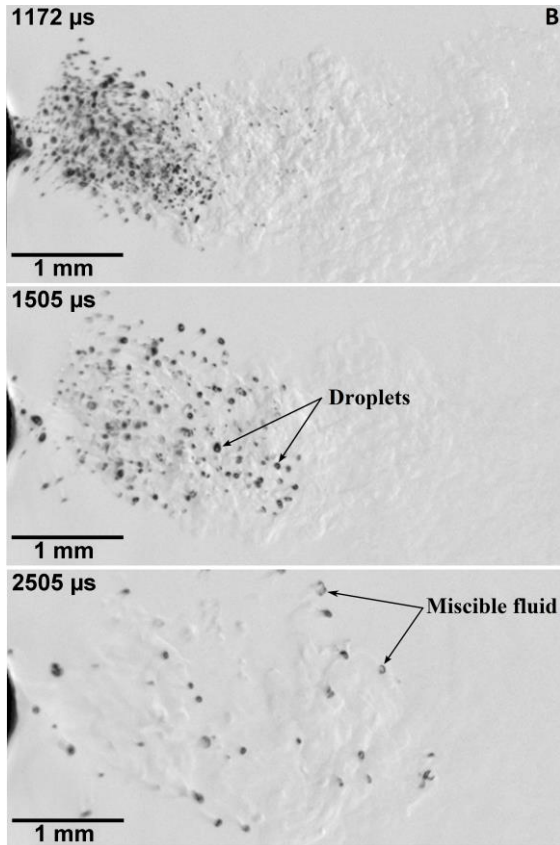
Figure 4. Time-sequences of the end of injection for n-hexadecane sprays at elevated pressures and temperatures. A- Spray breakup, droplet formation and classical droplet evaporation (900 K, 60 bar). B- Spray breakup, droplet formation and miscible mixing (1200 K, 105 bar).

The first aspect noticeable on these two sequences is the fewer number of features or droplets on the B-case of Figure 4. Another easily observable feature is the different vapor clouds in the spray stream, with more detectable "schlieren-like" patterns for the sequence of Figure 4B compared to Figure 4A. This could be attributed to the higher ambient density of the sequence in Figure 4B, but other effects may impact the response of the optical system in such a way, as pointed out by Falgout et al. [7]. Looking more closely to the features and tracking them on the high-speed movies reveal fundamentally different processes: Figure 4A shows ligaments transforming or disintegrating into droplets of spherical shapes and reducing in size until they are no longer detected by the imaging system. Figure 4B also shows ligaments breaking up into droplets near the nozzle (first image of the sequence), but the initially spherical droplets do not reduce in size and disappear like in the case of Figure 4A, rather the fluid structures deform and break into multiple non-spherical fluid parcels.

The sequence visible in Figure 4A is an example of classical evaporation process, where the droplets heat up and vaporize on the surface, to eventually get smaller and smaller, until all the liquid is evaporated. The images of Figure 4B also show classical evaporation, but another process enhances liquid – gas mixing by deforming and breaking the droplets into smaller parcels, which quickly disappear into the ambient gases. It is important to note that both these conditions present pressures and temperatures well above the critical point of the injected fuel (n-hexadecane: p_{cr} = 14.3 bar, T_{cr} = 722 K [10]).

Such mixing processes present contrasting differences with the classical view of liquid spray mixture formation with the surrounding gases. Based on the analysis provided by Dahms and coworkers [1, 8], the high ambient pressure and temperature under these conditions broadens the interface between a droplet and the surrounding gas. The elevated pressures and temperatures of the ambient gases impact the intermolecular forces of the injected fluid (liquid), thus reducing interfacial forces (surface tension) to minimal levels such that the droplets break into multiple subscale entities. The first fundamental impact is that the mixing rate can be substantially enhanced compared to the classical droplet vaporization process, as shown later. It is still early to comment on the impact of miscible mixing on the global mixing field when operating conditions are varied, but future works will attempt at quantifying droplet lifetime across the different ambient conditions typical of diesel engines, as detailed further in this document.

Nevertheless, it is possible to observe the impact of fuel on spray formation and mixing processes in the near-nozzle region at elevated temperature and pressure. Figure 5 shows image sequences of the end of injection for three alkane fuels: n-hexadecane, n-dodecane and n-heptane. These three fuels are typical surrogates used in laboratory experiments simulating diesel engine combustion. The injector is located right on the left edge of the images, and the ambient conditions are the same for all three sequences: 1200 K, 105 bar, to highlight the impact of fuel. The timings presented in Figure 5 are equal for all three sequences and are related to the start of injection. As such, the relationship with end of injection is expected to be similar, but not identical because of the different fuel properties; viscosity for instance is known to affect the hydraulic performance of the injector. The potential timing difference is not expected to affect the conclusions drawn from these sequences. The optical resolution of the system has been enhanced from Figure 4: The digital reso-

lution of the images is 2.5 µm/pix; the field of view being reduced to approximately 2 mm in length, or less than half that of Figure 4. The MTF for this configuration is plotted in Figure 3 (8x curve) for comparison with the previous setup.
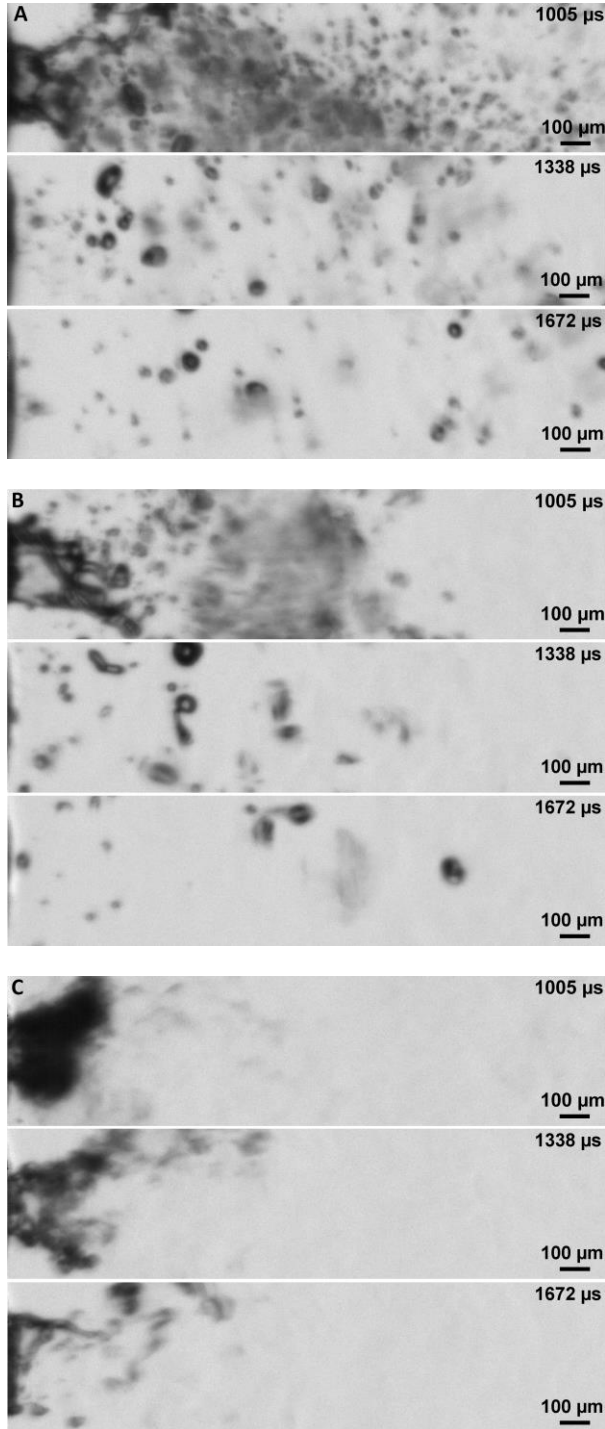
**Figure 5**. Time-sequences of sprays during the end of injection for different fuels at chamber target pressures and temperatures of 10.5 MPa and 1200 K, respectively. A- N-hexadecane. B- N-dodecane. C- N-heptane.

Increasing imaging magnification reveals details about the transition from classical evaporation to miscible mixing, emphasizing the drastic reduction of intermolecular forces (surface tension), and thus allowing the fluid to mix with the ambient gases via diffusion. As for Figure 4, these observations can hardly be made from image sequences and must be made from the high-speed movies. Nevertheless, the information visible on the still images showed in Figure 5 highlight the effect of fuel, under an ambient condition considered transcritical for the three fuels tested. Cross-comparison of the fuel image sequences with respect to time shows that droplets and ligaments are generated for both n-hexadecane and n-dodecane, but no cohesive liquid structures (ligaments or droplets) can be identified in the n-heptane case. Moving further in time, similarities are evident between n-hexadecane and n-dodecane, with droplets featuring a bright region in the center because of the refraction of light. Note that light refraction within the droplet was also observable on the images of Figure 4, but the magnification level of Figure 5 offers a clear view on such aspect. The fact that no spherical fluid structures or droplets featuring refraction patterns can be seen in the n-heptane case suggests that the interaction between light and fluid parcels is different from the other two fuels. The fluid properties between the three alkanes shown in Figure 5 are different because of the chemical composition (number of carbon atoms, from 16 to 7). As such, these three sequences show fluid mixing processes for fuels ranging from a heavy hydrocarbon fuel (n-hexadecane), to a lighter fuel (n-heptane). The critical points of these fuels are also different [10], which certainly provides additional explanations for the observations made on Figure 5. In all three cases, the ambient pressure is at least three times the critical pressure. Temperature is more complicated because of the transcritical process, the fluid being injected below the critical temperature into an ambient above this point. The lower critical temperature of n-heptane (540 K) compared to the other two fuels may accelerate interface broadening and reduce the time to transition from compressed liquid to miscible fluid.

Based on the observations extracted from the high-speed movies shown as image sequences in Figure 4 and 5, it has been demonstrated that the injection and mixing processes under such pressure and temperature conditions result in miscible mixing with reduced surface tension. This transition to a miscible fluid occurs at different times after the fluid parcel has been injected, as shown in Figure 4. This means that classical evaporation and miscible mixing may coexist at the same

time under certain conditions. The results of Figure 5 bring another aspect with the case of n-heptane, in which no ligaments or droplets can be observed, contrasting with the other two fuels and what has been seen in Figure 4. This condition suggests that the transition to miscible mixing can be very fast, on the order of a few microseconds. As such, the fluid intermolecular forces are diminished as soon as the fluid enters the chamber and the features easily detected at the end of injection do not exhibit signs of surface tension. It is important to note that the analysis above is for the end of injection period and other effects may be present during the main period of the injection event where the fluid enters the chamber at greater velocity. While the main period of injection is more difficult to analyze because of faster moving structure and optically thick sprays, future works will seek more clarity about the transition to miscible mixing in these environments.

Focusing on sample droplets under high temperature conditions highlights the differences between classical evaporation and miscible mixing. The time-resolution of the experiments allows tracking and following individual features (droplets or fluid blobs), especially at the end of the injection, when the flow becomes slower and the lifetime of the features detectable by the imaging system gets longer. Even though Figure 5 made the distinction between the evidence of surface tension, or not, a direct comparison between classical evaporation and the transition to miscible mixing is needed. Figure 6 presents image sequences centered on two sample droplets (fluid structures) under the two "vaporization" processes identified above. The sequence of Figure 6A follows a droplet featuring classical evaporation, where the droplet reduces in size until it is no longer detected by the optical instrument. The other image sequence (Figure 6B) shows how a structure evolves to transition into miscible fluid, where surface tension forces can no longer compete with the aerodynamic forces surrounding the fluid structure. N-hexadecane fuel is initially injected at the same temperature of 363 K, and at an injection pressure of 50 MPa for both sequences. The ambient conditions are the same as those presented in Figure 4: 60 bar, 900 K, for Figure 6A, and 1200 K, 105 bar, for Figure 6B.
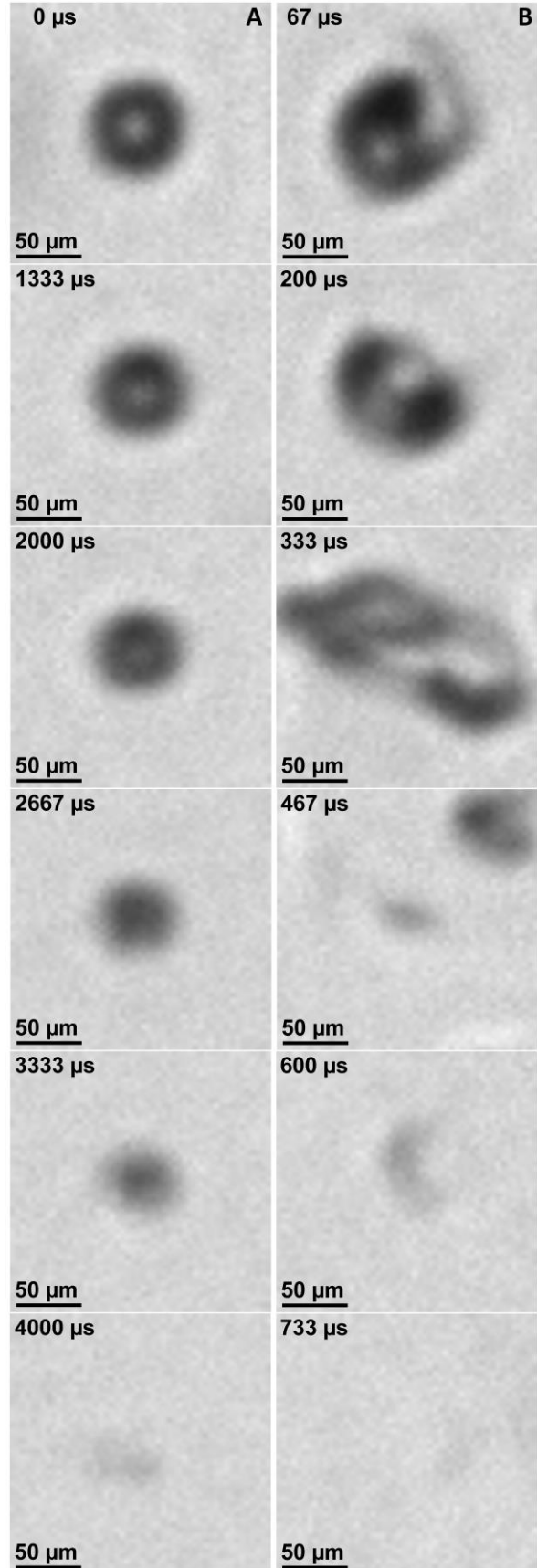
Figure 6. Time-history of n-hexadecane droplets featuring different mixing processes. A- Classical evaporation (900 K, 60 bar). B- Miscible mixing (1200 K, 105 bar).

The classical viewpoint on droplet evaporation is well understood, and numerous models, adding more or less complexity to the process can be used to describe the evolution of droplet size with time. The current knowledge regarding droplet vaporization states that the mass is transferred from the liquid parcel to the gas on the surface of the drop. Detailed numerical simulations suggest that the mass transfer within the drop due to convection plays a role in the mean temperature of the drop and its distribution [11]. If accuracy of the predictions is required, the vaporization model must include many parameters, some of which can be particularly difficult to measure, such as the temperature of the gas surrounding the droplet, or the relative slip velocity (velocity difference between the droplet and the gas). These parameters impact the vaporization process significantly and research is still ongoing to leverage our understanding of the physics in order to generate accurate models under droplet vaporizing in turbulent flows with high temperature differences.

The sequence shown in Figure 6B presents a different behavior, as has been described in previous figures. The detailed visualization and tracking of a single fluid structure undergoing transition to miscible mixing really demonstrates the different mass transfer between the compressed liquid phase to the miscible fluid phase (supercritical fluid). The droplet does not reduce in size as shown in Figure 6A, but deforms as it is subjected to aerodynamic forces, while intermolecular forces are weakened. Under shear and stress, the fluid structure stretches and breaks into multiple fluid parcels, as mentioned about the images shown in Figure 4. An important parameter to look at is the time it takes for a droplet to vaporize, compared to the time for this breakup and transition to occur. In fact, in the present example (Figure 6A), it takes over five times longer for the droplet to reduce in size until it is no longer visible, compared to the time it takes the fluid structure to stretch and break until it disappears (Figure 6B). It is true that the conditions are different and that the residence time of both droplets until the beginning of the image sequences presented in Figure 6 are different. Nonetheless, even taking these differences into account, it seems like the phase transition from liquid to gas or dense fluid happens faster under conditions where miscible fluid mixing is observed. Further investigation is needed to quantify the difference in "evaporation" rates between the classical evaporation scheme and the transition to miscible fluid. Again, such information and accompanying analysis will always be affected by the lack of knowledge regarding surrounding gas temperature of droplet relative velocity.

Summary and conclusions

Detailed measurements of the mixing processes of liquid fuel sprays at high temperatures and high pressures have been performed. Long-working-distance microscopy has been used in conjunction with high-speed imaging to track individual fluid features until they were no longer detected by the instrument.

The experimental data revealed that a different mechanism of "droplet evaporation" occurred at elevated pressures and temperatures. This phenomenon regarding the mixing of the fuel with the ambient is analogous to the miscible mixing process observed in liquid rockets, when conditions are above the critical points of the fluids. Under the conditions simulated in these experiments, and relevant to thermal engine combustion, the process is transcritical, as the fuel enters the ambient at temperatures lower than the critical point. As it mixes with the ambient gases, the injected fluid heats up, and the combined effects of pressure and temperature reduces intermolecular forces until surface tension eventually vanishes. As such, the effects of surface tension on the fluid structures have been observed, along with both evaporation and miscible mixing under most engine-relevant conditions.

It has been seen that the transition from classical evaporation to miscible mixing was affected by the ambient conditions (temperature and pressure), the fuel properties and the droplet size (distribution). The timescale of the transition also seemed to be important as the temperature increase of fluid parcels requires certain amount of mixing (time). For some particular conditions though, surface tension appeared to be negligible as its effects could not be directly observed.

Future works will concentrate on extracting information regarding droplet lifetime and the impact of miscible mixing on the global mixing process of vaporizing/combusting spray systems.

References

[1] R. N. Dahms, J. Manin, L. M. Pickett, and J. C. Oefelein. Understanding high-pressure gas-liquid interface phenomena in diesel engines. *Proceedings of the Combustion Institute*, 34(1):1667–1675, 2013.

[2] Engine Combustion Network. www.sandia.gov/ecn/. *Sandia National Laboratories*, 2009.

[3] L. M. Pickett, J. Manin, C. L. Genzale, D. L. Siebers, M. P. M. Musculus, and C. A. Idicheria. Relationship between diesel fuel spray vapor penetration/dispersion and local fuel mixture fraction. *SAE Paper 2011-01-0686 - SAE Int. J. Engines*, 4(1):764–799, 2011.

[4] W. Mayer and H. Tamura. Propellant injection in a liquid oxygen/gaseous hydrogen rocket engine. *Journal of Propulsion and Power*, 12(6):1137–1147, 1996.

[5] R. N. Dahms and J. C. Oefelein. On the transition between two-phase and single-phase interface dynamics in multicomponent fluids at supercritical pressures. *Physics of Fluids*, 25:092103, 2013.

[6] J. Manin, M. Bardi, L. M. Pickett, R. N. Dahms, and J. C. Oefelein. Microscopic investigation of the atomization and mixing processes of diesel sprays injected into high pressure and temperature environments. *Fuel*, 134:531–543, 2014.

[7] Z. Falgout, M. Rahm, Z. Wang, and M. Linne. Evidence for supercritical mixing layers in the ecn spray a. *Proceedings of the Combustion Institute*, 35(2):1579–1586, 2015.

[8] R. N. Dahms and J. C. Oefelein. Non-equilibrium gas–liquid interface dynamics in high-pressure liquid injection systems. *Proceedings of the Combustion Institute*, 35(2):1587–1594, 2015.

[9] M. Meijer, B. Somers, J. Johnson, J. Naber, S.-Y. Lee, L.-M. Malbec, G. Bruneaux, L. M. Pickett, M. Bardi, R. Payri, and T. Bazyn. Engine Combustion Network (ECN): characterization and comparison of boundary conditions for different combustion vessels. *Atomization and Sprays*, 22(9):777–806, 2012.

[10] E. W. Lemmon and A. R. H. Goodwin. Critical properties and vapor pressure equation for alkanes CnH2n+2: Normal alkanes with n < 36 and isomers for n = 4 through n = 9. *Journal of Physical and Chemical Reference Data*, 29(1):1–39, 2000.

[11] B. Duret, M. Al Qubeissi, S. Sazhin, and C. Crua. Evaporating droplets: comparisons between DNS and modelling. *ILASS-Europe 2014, Bremen, Germany*, 2014.